Am J Physiol Heart Circ Physiol 326: H370–H384, 2024.
First published December 8, 2023; doi:10.1152/ajpheart.00562.2023

american physiological society

AMERICAN JOURNAL OF PHYSIOLOGY
HEART AND CIRCULATORY PHYSIOLOGY

RESEARCH ARTICLE

Sarcomere, Cytoskeleton, and Mechanobiology Research

Differential sensitivity to longitudinal and transverse stretch mediates transcriptional responses in mouse neonatal ventricular myocytes

Shulin Cao,[1] Kyle S. Buchholz,[1] Philip Tan,[3] Jennifer C. Stowe,[1] Ariel Wang,[1] Annabelle Fowler,[1] Katherine R. Knaus,[1] Ali Khalilimeybodi,[4] Alexander C. Zambon,[5] Jeffrey H. Omens,[1,2] Jeffrey J. Saucerman,[3] and Andrew D. McCulloch[1,2]

[1]*Department of Bioengineering, University of California San Diego, La Jolla, California, United States;* [2]*Department of Medicine, University of California San Diego, La Jolla, California, United States;* [3]*Department of Biomedical Engineering, University of Virginia, Charlottesville, Virginia, United States;* [4]*Department of Mechanical and Aerospace Engineering, University of California San Diego, La Jolla, California, United States; and* [5]*Department of Biopharmaceutical Sciences, Keck Graduate Institute, Claremont, California, United States*

Abstract

To identify how cardiomyocyte mechanosensitive signaling pathways are regulated by anisotropic stretch, micropatterned mouse neonatal cardiomyocytes were stretched primarily longitudinally or transversely to the myofiber axis. Four hours of static, longitudinal stretch induced differential expression of 557 genes, compared with 30 induced by transverse stretch, measured using RNA-seq. A logic-based ordinary differential equation model of the cardiac myocyte mechanosignaling network, extended to include the transcriptional regulation and expression of 784 genes, correctly predicted measured expression changes due to anisotropic stretch with 69% accuracy. The model also predicted published transcriptional responses to mechanical load in vitro or in vivo with 63–91% accuracy. The observed differences between transverse and longitudinal stretch responses were not explained by differential activation of specific pathways but rather by an approximately twofold greater sensitivity to longitudinal stretch than transverse stretch. In vitro experiments confirmed model predictions that stretch-induced gene expression is more sensitive to angiotensin II and endothelin-1, via RhoA and MAP kinases, than to the three membrane ion channels upstream of calcium signaling in the network. Quantitative cardiomyocyte gene expression differs substantially with the axis of maximum principal stretch relative to the myofilament axis, but this difference is due primarily to differences in stretch sensitivity rather than to selective activation of mechanosignaling pathways.

NEW & NOTEWORTHY Anisotropic stretch applied to micropatterned neonatal mouse ventricular myocytes induced markedly greater acute transcriptional responses when the major axis of stretch was parallel to the myofilament axis than when it was transverse. Analysis with a novel quantitative network model of mechanoregulated cardiomyocyte gene expression suggests that this difference is explained by higher cell sensitivity to longitudinal loading than transverse loading than by the activation of differential signaling pathways.

cardiac myocyte; mechanosignaling network; network model; stretch; transcriptional regulation

INTRODUCTION

In the heart, hemodynamic overload can induce different modes of ventricular hypertrophy and remodeling (1) associated with different mechanical stimuli (2, 3). Several cell signaling pathways and mechanisms have been implicated in the myocyte hypertrophy response to mechanical loading and stretch (4–6), but little is known about the specific pathways and mechanical stimuli that mediate predominant myocyte lengthening during ventricular volume overload versus myocyte thickening in response to ventricular pressure overload (7). The internal organization of the sarcomere and cytoskeleton suggests that myocytes may respond differentially to loading applied either parallel or transversely to the long axis of the cell. In micropatterned, elongated neonatal rat cardiac myocytes, phenotypic responses to 24 h of static stretch differed significantly when stretch was applied primarily along the cell axis compared with transverse to it (8, 9).

Previous studies have shown that longitudinal uniaxial stretch of aligned neonatal rat ventricular myocytes induced the addition of new sarcomeres in series so that, by 6 h, the

Correspondence: A. D. McCulloch (amcculloch@ucsd.edu).
Submitted 11 September 2023 / Revised 29 November 2023 / Accepted 29 November 2023

original unstretched sarcomere length had been restored (10). Hence, the hypertrophic signaling and remodeling responses to stretch in neonatal myocytes in vitro are likely quite rapid. Many studies have also shown evidence of paracrine and autocrine responses to stretch that act over short- and long-term time scales (11). Therefore, the first goal of this study was to examine the differential gene expression profiles following up to 4 h of stretch in micropatterned neonatal mouse cardiac myocytes and compare responses when the cells are stretched primarily along or transverse to their long axes.

To elucidate the signaling pathways regulating differential transcriptomic responses to stretch, a second goal of this study was to expand our previous logic-based computational model of the cardiac myocyte mechanosignaling network (12) by incorporating transcriptional control of 784 genes regulated by the 11 transcription factors (TFs) in the network. In the signaling model, stretch activates pathways downstream of mechanically sensitive membrane receptors and channels. Differential gene expression predicted by the model showed 69% agreement with measured gene expression after 4 h of longitudinal stretch and 72% agreement with genes that were significantly changed after stretch. We used the model to predict the sensitivity of gene expression to the activation of different membrane receptors and ion channels and then validated these findings with receptor and channel blocking experiments in vitro. Combining experimental data and model analysis, these findings suggested that the observed differences between myocyte transcriptional responses to transverse and longitudinal stretch were not explained by differential activation of specific pathways but rather by substantially greater myocyte mechanosensitivity to longitudinal stretch than transverse stretch.

MATERIALS AND METHODS

Cardiomyocyte Isolation, Micropatterning, and Culture

Cardiac myocytes were cultured on flexible, micropatterned elastomeric substrates and subjected to a static mechanical load using methods described previously (13). In brief, Sylgard 186 polydimethylsiloxane (PDMS) membranes were spin coated on silicon wafer master molds micropatterned with SU-8 2005 negative photoresist using a custom photomask, degassed, and cured at 70°C for 30 min and at room temperature overnight. The resulting 10-μm-wide microgrooves were 5 μm deep and 10 μm apart. The micropatterned membranes were mounted in custom elliptical cell stretchers, and murine laminin was adsorbed under 350-nm wavelength radiation at 10 μg/mL in phosphate-buffered saline (PBS). Excess protein was removed by rinsing twice in 1X PBS before plating cells.

Cardiac myocytes were isolated as an aggregated cell pool from the hearts of 1- to 2-day-old (P1–P2) C57BL/6 mouse pups (Charles River Labs) of both sexes as described previously (14). Cells were divided into experimental groups and technical replicates of approximately equal cell number and plated on the micropatterned PDMS membranes in the stretchers at a density of 1.5–2 million cardiac myocytes in an area of ~600 mm^2 per stretcher. Cell media consisted of Dulbecco's modified Eagle medium and Medium-199 supplemented with 10% horse serum, 5% fetal bovine serum, 10 mM HEPES buffer, 100 U/mL penicillin, and 100 μg/mL streptomycin and incubated at 37°C with 5% CO_2. At 72 h after plating, media were changed to a serum-free media, and the cells were cultured for another 24 h before stretch, taking on an aligned, rod-like morphology (8).

Cell Stretch and Expression Profiling

The elliptical stretchers applied an anisotropic, biaxial strain of 14% to the membrane along the minor axis of the ellipse and 3.6% along the major axis (8) to the cultures. Membranes were oriented during assembly into the stretchers so that myofiber alignment would be parallel either to the minor axis of the ellipse (producing primarily longitudinal stretch) or to its major axis (transverse stretch). Cultures were stretched statically for 30 min or 4 h, and control cultures were micropatterned on the same engineered substrates, assembled into the stretch device, but not subjected to stretch, for a total of four test groups and one control group. Three stretchers for each condition served as technical replicates. Total RNA was extracted using RNeasy Mini Kit.

Total RNA samples were tested for quality using an Agilent Technologies 2100 Bioanalyzer. RNA samples were prepared for sequencing with the TruSeq RNA Sample Prep Kit v2 according to the manufacturer's instructions and then single-end sequenced with an Illumina HiSeq 2000. Quality analysis was performed using FastQC (15). Low-quality reads and adapter sequences were trimmed with FASTQ trimmer in the FASTX-Toolkit (Supplemental Fig. S1; Supplemental Materials are available at https://doi.org/10.5281/zenodo.10247058) (A. Gordon and G. Hannon, unpublished observations), aligned to mm9 mouse genome with HiSat2 (16). Feature counts were used to count aligned reads, and DESeq2 (RRID:SCR_015687) was used to test for differential expression by comparing abundance of gene expression in each experimental condition with control (17, 18). RNA-seq data were deposited in GEO (Accession No. GSE83655). Genes with a false discovery rate (FDR) <0.05 and a minimum $\log_2$ fold change (FC) of 0.5 with respect to control were defined as differentially expressed. See *Statistical Analysis*.

Reverse transcription polymerase chain reaction (RT-PCR) was used to validate representative RNA-seq results and for receptor blocking experiments. RNA was quantified using Qubit 2.0 and the Qubit Broad-Range RNA Kit or NanoDrop RNA quantification settings. cDNA synthesis was performed using an RNA input of 500 ng per reaction and a ProtoScript First Strand cDNA Synthesis Kit (New England Biolabs). Reverse transcription polymerase chain reaction (RT-PCR) was performed on a Life Technologies StepOnePlus Real-Time PCR System using a KAPA SYBR Fast Universal qPCR kit. Glyceraldehyde-3-phosphate dehydrogenase (GAPDH) or 18S ribosomal RNA are both housekeeping genes used as the reference gene for fold change normalization. Primers for RT-PCR are listed in Supplemental Table S1. Neonatal ventricular myocytes used for RNA-seq and PCR validation measurements of all experimental groups and replicates were isolated and pooled from a single batch of hearts from 101 P1–P2 C57BL/6 mouse pups of both sexes from eight litters.

Pathway Enrichment Analysis

Functional and pathway enrichment analyses were performed by comparing differentially expressed genes with the Gene Ontology (GO) and Kyoto Encyclopedia of Genes and Genomes (KEGG) database. Differentially expressed genes were categorized into lists of upregulated or downregulated genes for each stretch condition. These lists were analyzed with DAVID (19), which identified enrichment of genes in pathways and gene ontologies (20). The criteria for classifying a term as enriched were false discovery rate (FDR) <0.05 and number of differentially expressed genes annotated with the term >2.

Inhibition Studies of Mechanosensitive Receptors

To test the predictions of the network model, cultured myocytes were stretched with and without combinations of pharmacological inhibition of membrane receptors in the following three treatment groups: *1*) angiotensin II type 1 (AT_1) receptor inhibition with 1 μM losartan 4 h before stretch followed by endothelin type A and type B receptor inhibition with 100 μM BQ123 and 10 μM BQ788, respectively, both added 30 min before stretch; *2*) mechanosensitive ion channel (including Trp and PIEZO) blockade with 1 μM ruthenium red (21), L-type calcium channel (LTCC) blockade with 5 μM nifedipine, and sodium hydrogen exchange (NHE) channel blockade with 10 μM HOE642 (cariporide), all applied 10 min before stretch; *3*) a control group receiving the vehicles used in *groups 1* and *2* containing 2 μL double-distilled water (ddH_2O) added 4 h before stretch, followed by 50 μL ddH_2O and 2 μL dimethyl sulfoxide (DMSO) 30 min before stretch and 2 μL ddH_2O and 4 μL dimethyl sulfoxide (DMSO) added 10 min before stretch. Chemical compounds were purchased from MilliporeSigma and R&D Systems. Half the cultures in each group were stretched (14% transversely and 3.6% longitudinally), and half were not stretched (control). All cultures were incubated for 4 h at 37°C, 10% CO_2, and 100% humidity. All compounds remained in culture during stretch. Cells were then rinsed with room temperature 1X PBS and lysed using Qiagen's RNeasy Mini Kit (Cat. No. 74104) following the standard protocol with β-mercaptoethanol in the RLT buffer. Neonatal ventricular myocytes used for all groups and replicates in these inhibitor experiments were isolated and pooled from a single batch of hearts from 20 neonatal mice of both sexes.

Timing, Frequency, and Handling

Samples from independent experiments (RNA-seq, PCR validation, and inhibitor studies) were each run as one large experiment on the same day at the same time of day. All replicates were treated the same way, including control stretchers, which were removed from the incubator and handled to mimic the manipulation that occurred when applying stretch to the stretched groups.

Mechanosignaling Network Model

To investigate the roles of different mechanosignaling pathways in regulating changes in gene expression in response to anisotropic stretch of ventricular myocytes, we extended our previously described computational model of the cardiomyocyte mechanosignaling network (12) to include transcriptional regulation and expression of genes downstream of the transcription factors in the network. Seven classes of nodes are represented in the expanded network model (Fig. 1), which was rendered with the aid of Cytoscape version 3.7.1 (RRID:SCR_003032) (22): 9 mechanoregulated ligands and membrane receptors; 4 canonical signaling pathways (calcium, MAPK, PI3K-Akt, and cytoskeletal related); 11 transcription factors that regulate 784 target genes and 14 of which code for proteins in the network itself. For clarity, we have only shown the transcriptional regulation of the 14 genes in the model that provide feedback to the network itself. These transcriptional regulatory reactions are new in the model, as is the feedback of their products to the network. The other 770 genes in the model and their transcriptional regulatory reactions, as well as the two hypertrophic phenotype outputs (cell area and protein synthesis) described in the original signaling model (12), have been omitted from Fig. 1 for clarity. Complete lists of genes, model reactions, and abbreviations for node names are provided in Supplemental Table S2.

As in our original cardiomyocyte mechanosignaling network model (12), signaling dynamics were modeled using differential equations with continuous logical operators. The activity of each species was normalized between 0 and 1 and followed a Hill-type sigmoidal function, as described previously (23). Constant default parameter values for weight ($w = 0.9$), Hill coefficient ($n = 1.4$), and half-maximal activation ($EC_{50} = 0.5$) were used for all reactions. For all reactions except transcription and translation reactions, a time constant τ of 0.5 min was assumed (see Supplemental Table S2). This time constant allows ERK1/2 and p38 MAPK to reach peak activation after 10 min of stretch, consistent with experimental observations (24).

Since gene transcription is conventionally and more easily normalized to control rather than maximal expression, a mass action method was used to model mRNA levels, $[mRNA_i]$, making use of mRNA degradation rates τ_i computed from mRNA half-lives, $\tau_{1/2}(i)$, that have been previously measured (25):

$$\tau = \frac{t_{1/2}(i)}{\ln 2}.$$

Stimulated messenger RNA transcription rates were then scaled by the transcriptional activation H_i of each output gene i as a function of transcription factors T_j of the network normalized to baseline activity H_i (T_0), while satisfying the assumption that measured baseline mRNA levels, $[mRNA_i]_0$, were all at steady state:

$$\frac{d[mRNA_i]}{dt} = \frac{1}{\tau_i} \times \frac{H_i\left(\sum_j a_j \times T_j\right)}{H_i(T_0)} \times \left([mRNA_i]_0 - [mRNA_i]\right),$$

where $H_i\left(\sum_j a_j \times T_j\right)$ represents the combined effects of upstream transcriptional regulators T_j of gene i on mRNA transcription and a_j are the weights on each transcription factor determined by the upstream network (23). In this formulation, the molar transcriptional rate for each mRNA is a function of transcriptional activation and mRNA levels (26).

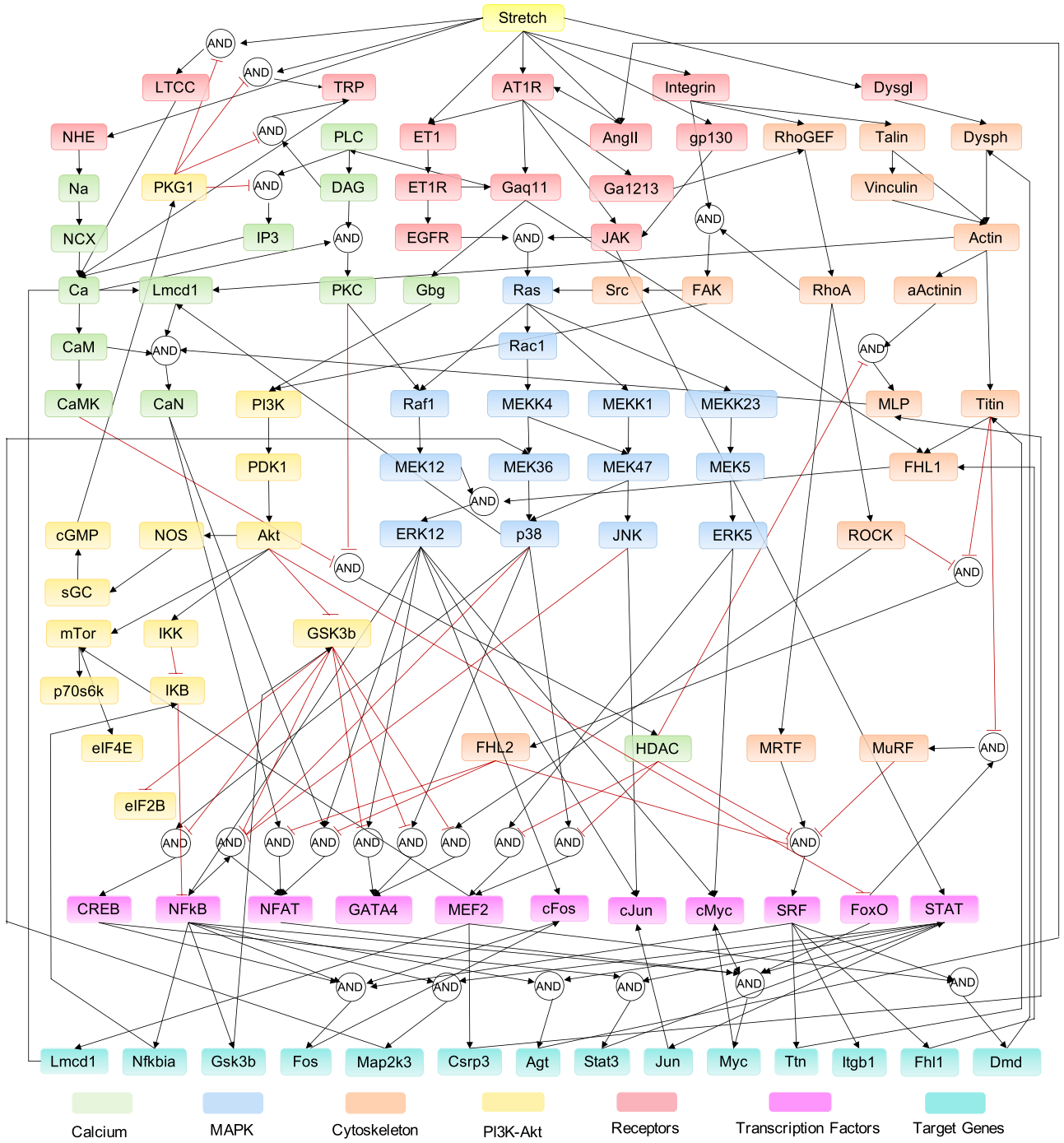

Figure 1. Reconstruction of the mechanosignaling network in cardiac myocytes. The model comprises 921 activating or inhibitory reactions linking mechanical stretch (lemon) to 84 signaling nodes downstream of ligands and receptors (red) via 4 signaling cascades (green, blue, orange, and yellow) and 11 transcription factors (pink) to 784 genes. For clarity, we only depict the transcriptional regulation of 14 genes (teal) coding nodes of the signaling network itself and the corresponding feedback representing protein translation and expression. See Supplemental Table S2 for a complete list of nodes, abbreviations, and reactions in the model.

The transcriptional regulatory model determining $H_i(T)$ has 11 transcription factor inputs: nuclear factor κ-light-chain-enhancer of activated B cells (NF-κB); nuclear factor of activated T cells (NFAT); signal transducer and activator of transcription (STAT); myocyte enhancer factor-2 (MEF2); serum response factor (SRF); cyclic adenosine monophosphate response element binding (CREB); cJun and cFos that heterodimerize to the early response factor AP-1; cellular Myc (cMyc); GATA-binding protein 4 (GATA-4); and forkhead transcription factors (FoxO), the only negative regulators of myocyte hypertrophy in the model. We identified 784 candidate target genes that were also detected in our RNA-seq measurements as having a binding site for 1 of the 11 transcription factors using iRegulon (27) with position

weight matrices from TRANSFAC (28), JASPAR (29), and UNIPROBE (30). Of these, transcriptional regulation has been confirmed experimentally for 288 genes by coexpression experiments in mice or rats, and 561 genes have been validated in published analyses of ChIP-seq datasets in mice or rats (see Supplemental Table S2). About 784 reactions were added to the original network model to approximate the transcriptional regulatory network (Supplemental Table S2, *rows 126–909*). Coregulation of the expression of 120 genes in the network was modeled using 144 AND operators, as shown in detail in Supplemental Table S2, *rows 126–909*. Finally, 14 target genes encode for an upstream protein in the mechanosignaling network itself. As a rudimentary representation of feedback due to translation and protein expression of these 14 genes, we scaled the protein node values by the relative activation of its corresponding gene assuming a gain of 0.33 (Supplemental Table S2, *rows 910–923*).

To estimate the baseline activation T_0 for each transcriptional regulator in the model, we first stimulated the mechanosignaling network model with an arbitrary baseline stretch input of 0.315 until a quasi-steady state was achieved. Unless otherwise stated, this initial input value was used to simulate all unstretched baseline conditions. Next, to determine the stretch input corresponding to the experimental stretch conditions, we regressed RNA-seq measurements against model-predicted mRNA counts for different stretch stimuli enforcing a zero intercept. For the case of longitudinal stretch applied to cardiomyocytes for 4 h, a stretch input of 0.7 to the model yielded a slope of 0.98 between $\log_2$ expression of measured versus simulated mRNAs (Pearson correlation between data and model, $r^2 = 0.969$). See Supplemental Fig. S2. Except where otherwise stated, this initial stimulus of 0.7 was used for all stretch simulations.

Fourteen gene outputs of the network were also coded for proteins in the network itself (Fig. 1). In lieu of using computed mRNA levels to simulate protein translation, the mRNA levels were renormalized to be consistent with the activation variable $H(T)$ and fed back to the signaling network instantaneously, since time constants for translation are typically small compared with those for transcription. Protein degradation was not modeled. Normalized mRNA output levels, $[\widehat{\mathrm{mRNA}_i}]$, were obtained from

$$[\widehat{\mathrm{mRNA}_i}] = \frac{[\mathrm{mRNA}_i]}{[\mathrm{mRNA}_i]_0} \times w \times H_i(T_0).$$

Network Centrality Analysis

Network centrality analysis (31) was used to find the most important nodes based on network topology (31). For a given network composed of multiple signaling nodes and pathways, a subnetwork can be formed between any two nodes of interest (starting point is defined as s and ending defined as e). The betweenness centrality is a function that assigns a numerical value to every node i in this subnetwork that monitors the communications between s and e (31, 32). Let σ_{se} denotes the number of shortest paths from s to e, then $b(i) = \sigma_{se}(i)/\sigma_{se}$ is the probability that this node i falls on the randomly selected shorted path between s and e (32). The betweenness centrality $C_B(i)$ of node i in the network is obtained by normalizing $b(i)$ to between 0 and 1:

$$C_B(i) = \frac{b(i) - b_{\min}}{b_{\max} - b_{\min}}.$$

The higher the centrality the greater the importance of this node in the subnetwork. For example, in a regulatory network beginning at the stretch stimulus and ending at the expression of a gene, if the betweenness centrality of a node in the network is 0.5, half of the pathway signals are transmitted to this node.

Numerical Implementation

The numerical computations used to simulate network dynamics were implemented in Python, and all the code, data, and numerical simulations used to generate results here are in a Jupyter Notebook publicly available on GitHub. See DATA AVAILABILITY.

Statistical Analysis

For analysis of differential gene expression, adjustments for multiple comparisons were performed using the false discovery rate (FDR) described by Benjamini and Hochberg (33). Power analysis was conducted on the RNA-seq data. To filter out genes with low expression, only genes with greater than 1 count for each sample were kept. The average number of counts per gene and the biological coefficient of variation for all genes were calculated using edgeR (34). These values along with an FDR of 0.05 and a minimum $\log_2$ fold change (FC) of 0.5 were taken as inputs into the R package rnaPower, which was used to calculate power (35). For statistically testing the significance of mRNA changes due to stretch measured by PCR and for comparing observed mRNA fold changes between RNA-seq and PCR, Student's t test was used with $P < 0.05$.

RESULTS

Transcriptome and Pathway Enrichment Analysis

The primary principal stretch axis was aligned either parallel (longitudinal stretch) or perpendicular (transverse stretch) to the cardiac myofibril orientation on the microgrooved substrates (Fig. 2*A*). The expression of 1,042 genes changed significantly compared with unstretched controls (FDR $\leq$ 0.05) under one or more stretch conditions (Supplemental Table S3). Of these significantly differentially expressed genes, $|\log_2 \mathrm{FC}| \geq 0.5$ for 562, including 557 after longitudinal stretch (40 after 30 min and 527 after 4 h) and 30 after transverse stretch (17 after 30 min and 13 after 4 h) (Fig. 2*B*). Hence, longitudinal stretch induced 99% of all differentially expressed genes in the experiment compared with the response to transverse stretch, which induced fewer than 5% of all genes differentially expressed in response to one or more stretch condition.

Cluster analysis of the 1,042 genes for which FDR $\leq$ 0.05 highlighted several distinct expression patterns (Fig. 2*C*). These include genes that were activated at 30 min and had returned to control levels by 4 h and genes that were induced at 30 min and remained activated at 4 h. Condition-wise clustering suggests that transverse stretch induced similar expression patterns to longitudinal stretch between 30 min and 4 h, whereas longitudinal stretch induced a greater

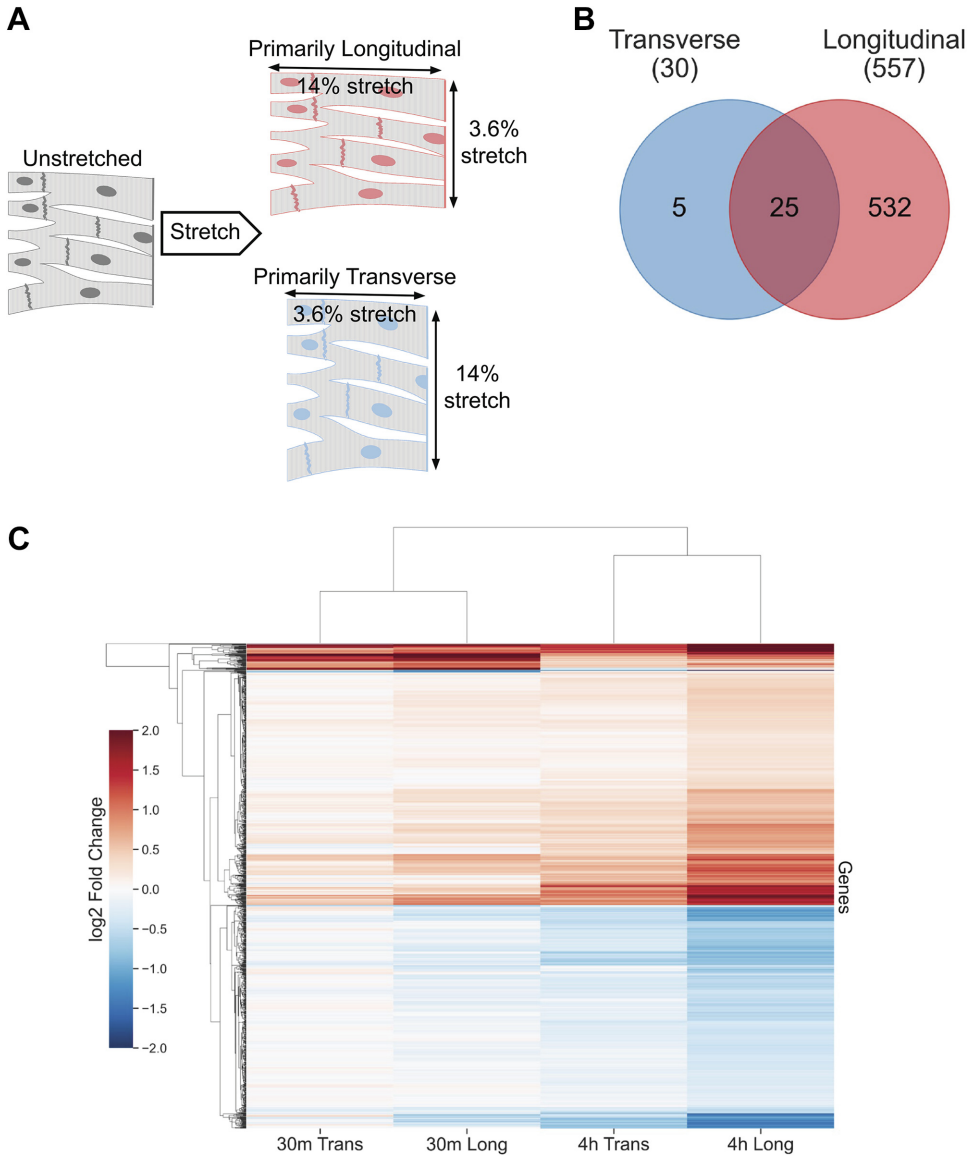

Figure 2. Differentially expressed genes in RNA-Seq measurements. *A*: schematic of myocyte stretch with orthogonal nonequibiaxial strains of 14 and 3.6%, showing stretch that is primarily longitudinal, in which the axis of 14% stretch is aligned longitudinally with the myofilament axis (*top*) or stretch that is primarily transverse to the myofilament axis (*bottom*). Stretches not shown to scale. *B*: Venn diagram of 562 genes differentially expressed (FDR $\leq$ 0.05 and $|\log_2 FC| \geq 0.5$) by transverse stretch (blue) or longitudinal stretch (red) for 30 or 240 min. *C*: clustering dendrogram (36, 37) of 1,042 differentially expressed genes (FDR $\leq$ 0.05) based on expression profiles using Pearson correlation with longitudinal stretch. Most genes change monotonically with time, but 5–10% displayed higher order dynamics. Results are mean $\log_2$ fold changes in mRNA abundance for each of the 4 stretch groups (30 min and 4 h each of transverse and longitudinal stretch) relative to mean mRNA abundance of the unstretched control group ($n = 3$ technical replicates for each of the 5 experimental groups). FC, fold change; FDR, false discovery rate.

response in gene expression compared with transverse stretch at both time points. Among these 1,042 genes, 60 were activated by 30 min of transverse stretch but then declined by 4 h, whereas these same genes were further activated by 4 h of longitudinal stretch. The expression of 33 genes changed significantly by 30 min but then reversed by 4 h for both stretch conditions. These genes displaying these higher order expression dynamics were confirmed to be immediate early genes.

RNA-seq measurements for differentially expressed genes representing each of these six clusters were validated using RT-PCR (Supplemental Fig. S3). The measurements agreed closely, with a Pearson correlation coefficient of 0.97, and differences between fold changes measured by RNA-seq or PCR were not statistically significant, though for three genes, the response to transverse stretch measured by PCR did not reach statistical significance compared with controls.

Figure 3 shows a subset of the KEGG pathways that were statistically enriched in the measured transcriptomic responses to stretch ordered from top to bottom by statistical significance. Among all the enriched pathways, genes associated with MAPK signaling were significantly enriched as early as 30 min. Differentially expressed genes enriched in the MAPK signaling pathway included many of the immediate early genes that segregated in the foregoing clustering analysis. Other pathways, such Ras signaling, the PI3K-Akt pathway, calcium signaling pathways, and regulation of actin skeleton, were enriched in the 4-h measurements (Fig. 3*A*). Most foundational pathways used to build the model (labeled in bold) were also enriched in the pathway analysis. For 26 of these 37 pathways, there was also significant enrichment of genes regulated by the network model (Fig. 3*B*).

Mechanosignaling Network Dynamics

Setting the baseline stretch input variable of the model to 0.315 until quasi-steady state constitutive activation of the network was achieved and then applying a stretch stimulus of 0.7 for 4 h induced gains on a $\log_2$ scale of −1.9 to 5.1 for gene outputs of the model that were also significantly

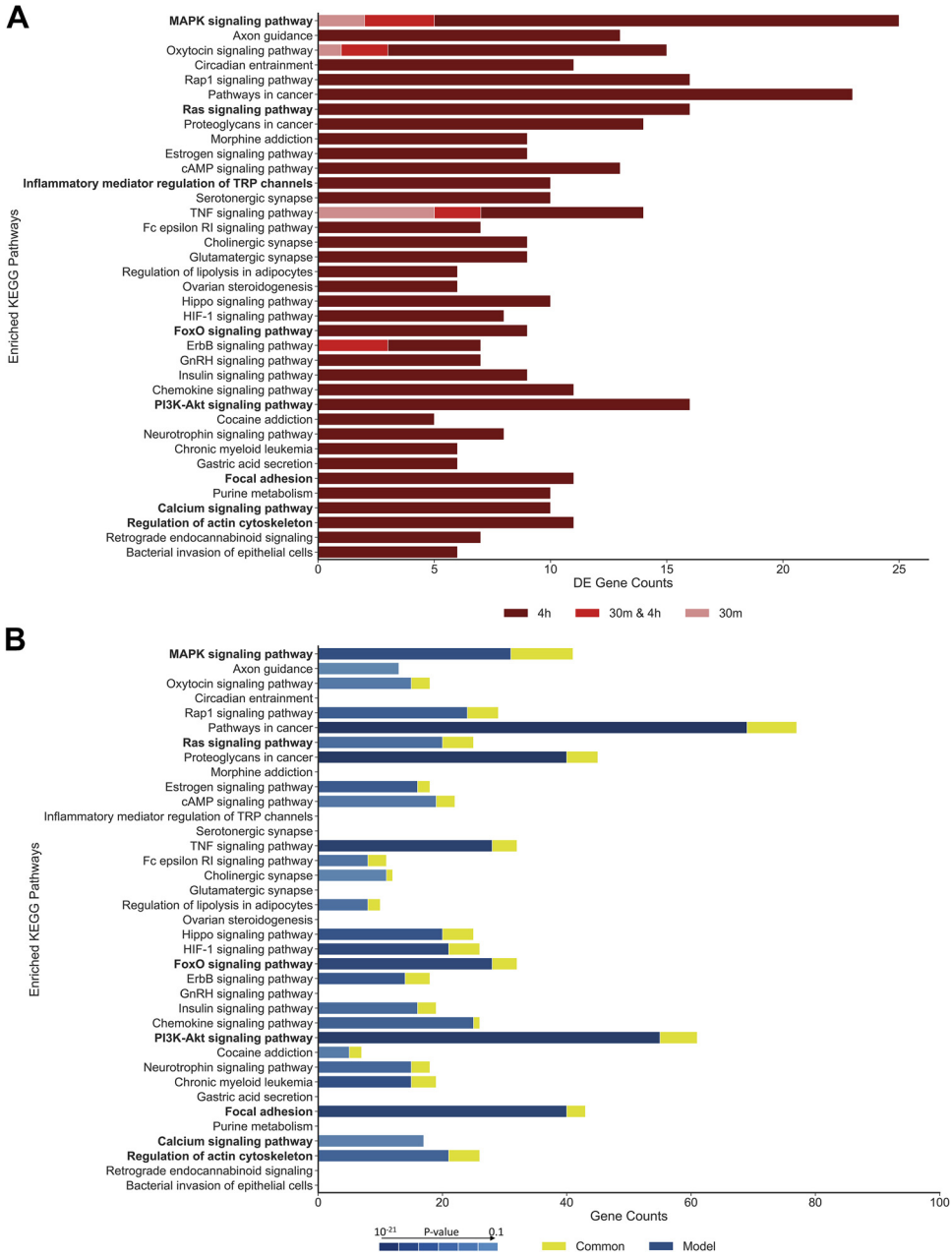

Figure 3. Kyoto Encyclopedia of Genes and Genomes (KEGG) pathway enrichment analysis. *A*: all pathways in the KEGG database for which 562 differentially expressed genes are statistically enriched ordered by statistical significance with most highly enriched pathways at the top. Bars show number of differentially expressed genes in each pathway: after stretch for 30 min (light red, 57 genes); 4 h (dark red, 540 genes); both 30 min and 4 h (red, 562 genes). Enrichment *P* values ranged from 3.6×10^{-7} to 4.7×10^{-2}. *B*: number of genes from enriched KEGG pathways in *A* of the 784 genes that are also in the network model: model genes that were not (blue) and were (yellow) differentially expressed. Pathways shaded based on statistical significance of enrichment with darkest colors for lowest *P* values (minimum, 4.7×10^{-21}) and lightest colors for highest *P* values (maximum, 0.08). Pathways labeled in boldface are also foundational networks of the signaling model.

differentially expressed by 4 h of longitudinal stretch in the experiments. The corresponding measured gains ranged from −2.0 to 2.8. Similarly, for gene outputs of the model that were significantly induced by transverse stretch, the model gains were −0.8 to 3.0 after 4 h compared with measured values in the range −2.5 to 1.5.

Figure 4 shows the change in expression of all 784 target genes during 12 h of model simulation, together with the time course of stretch stimulus. Since experimental studies (10) have shown that 10% static stretch of aligned neonatal ventricular myocytes induces the addition of sarcomeres sufficient to restore sarcomere length to prestretch values within 4 h, the apparent stretch felt by the cells dissipates over this time course. We simulated this decay with feedback from the cell area output variable of the model to the applied input stretch. By 4 h, cell growth caused the applied stretch input variable to decay by ∼80% of the difference between the initial value of 0.7 to the baseline (no stretch) value of 0.315. Each row in Fig. 4 corresponds to the expression time course of a different target gene, with the rows ordered by the net change in expression after 12 h. During this time course, 266 target genes increased with stretch and 46 targets decreased by more than the threshold $\log_2$ fold change of 0.5. Among the 266 upregulated genes, 101 reached a peak in expression before 12 h, and of the 46 downregulated genes, 28 reached a minimum. Varying the feedback due to transcriptional regulation of 14 nodes in the signaling network itself changed the model dynamics. Increasing the

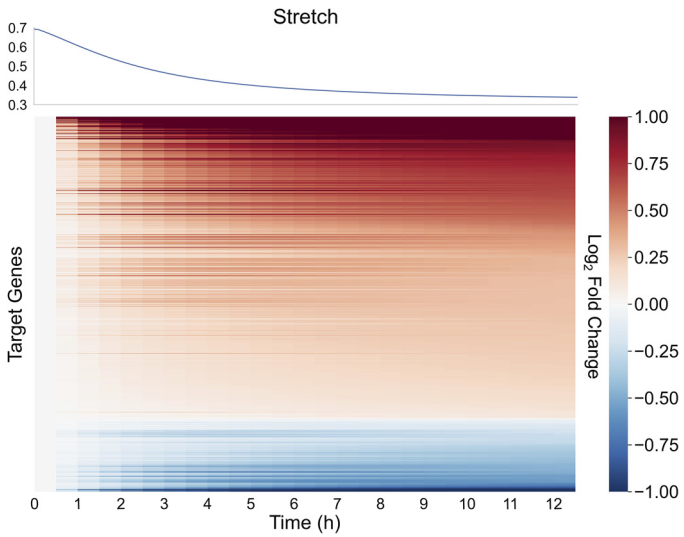

Figure 4. Model-predicted time course of gene expression in response to 12-h static stretch. Log_2 fold changes in expression of all target genes in the model during 12 h of simulated static stretch (*bottom*) in which feedback from the cell area output of the model decreases apparent cell stretch as myocytes hypertrophy to restore unstretched sarcomere length (*top*).

feedback gain of the simplified translation model from 0.33 resulted in more complex network dynamics. We did not attempt to optimize model parameters.

Comparing Model-Predicted Gene Expression with Experimental Measurements

Comparing model-predicted gene expression with measured fold changes at the statistical threshold (FDR $\leq$ 0.05) for differential expression in the experiments, we chose a numerical threshold on a log_2 scale of ±0.5 to define a gene output of the model as differentially expressed (see Supplemental Fig. S4). These criteria assigned the gene outputs of the model into nine categories in a 3 $\times$ 3 contingency table, of which three represent model results that correctly classify the experimental data (i.e., increased expression in both model and experiment, decreased expression in both model and experiment, or no change in both model and model). Percent accuracy was computed by dividing these correctly classified genes by the total number of genes in the model.

For all 784 output genes, the network model successfully predicted whether expression was significantly upregulated or downregulated or unchanged in response to our RNA-seq measurements following 4-h longitudinal stretch with 69% accuracy. For the subset of 288 model genes, for which transcriptional regulation has been confirmed by coexpression experiments, accuracy was 77% (Table 1). For further validation, we also compared model predictions with two published datasets. The model predicted changes in the expression of 697 genes (262 experimentally confirmed) following 1-h cyclic stretch of neonatal rat ventricular myocytes (38) with 91% (87%) accuracy. Simulating 48 h of mechanical overload, we predicted changes in gene expression after 2-day transverse aortic constriction (TAC) in mice (39) with 63–76% accuracy.

Differential Responses to Transverse and Longitudinal Stretch

Although the statistically significant transcriptional responses to transverse stretch were largely a subset of the longitudinal stretch response, we observed that the numerical differences in differentially expressed genes were primarily due to quantitatively higher changes in mRNA level induced by longitudinal stretch than transverse stretch. Regressing log_2 fold changes measured for all genes shows a strong correlation between expression induced by longitudinal stretch versus transverse stretch (Fig. 5), even including genes that were not significantly upregulated or downregulated. Regression analysis of genes that were significantly differentially expressed by either stimulus showed that fold change responses were significantly greater ($P \leq 0.05$) with longitudinal stretch than transverse stretch, both after 30 min (slope = 1.17, $R^2 = 0.98$) and after 4 h, when the ratio was higher (1.71, $R^2 = 0.90$). These results suggest that the differences between transcriptional responses of neonatal cardiac myocytes to transverse and longitudinal stretches may be explained in large part by a higher sensitivity to longitudinal stretch than transverse stretch than by activation of different mechanosignaling pathways as a function of principal stretch axis.

Using the unstretched constitutive baseline stimulus of 0.315 and including decay in strain due to cell growth modeled by feedback from the cell area output variable, we investigated whether differences in gene expression magnitudes induced by longitudinal and transverse stretch (Fig. 5) are consistent with a lower global sensitivity to transverse stretch. Figure 6 shows the predicted and measured correlations between transcriptional responses to longitudinal and transverse stretches for 30 min and 4 h when longitudinal and transverse stretches were assumed to be equivalent to input stretch stimuli of 0.7 and 0.4, respectively. Regression lines fitted to model predictions at 4 h (Fig. 6*A*) and 30 min (Fig. 6*C*) closely matched the experimentally measured relationships for genes in the model (Fig. 6, *B* and *D*). Therefore, for subsequent model validation and comparison, we assumed that transverse stretch corresponded to an initial stretch stimulus of 0.4.

Table 1. *Validation of model-predicted gene expression from 3 independent experiments*

	Longitudinal Stretch (4 h)		Cyclic Stretch (1 h)		TAC (2 Days)		Combined
	n	Accuracy, %	*n*	Accuracy, %	*n*	Accuracy, %	Accuracy, %
All model genes	784	69	697	91	740	63	74
Experimentally confirmed genes	288	77	262	87	269	76	80

TAC, transverse aortic constriction.

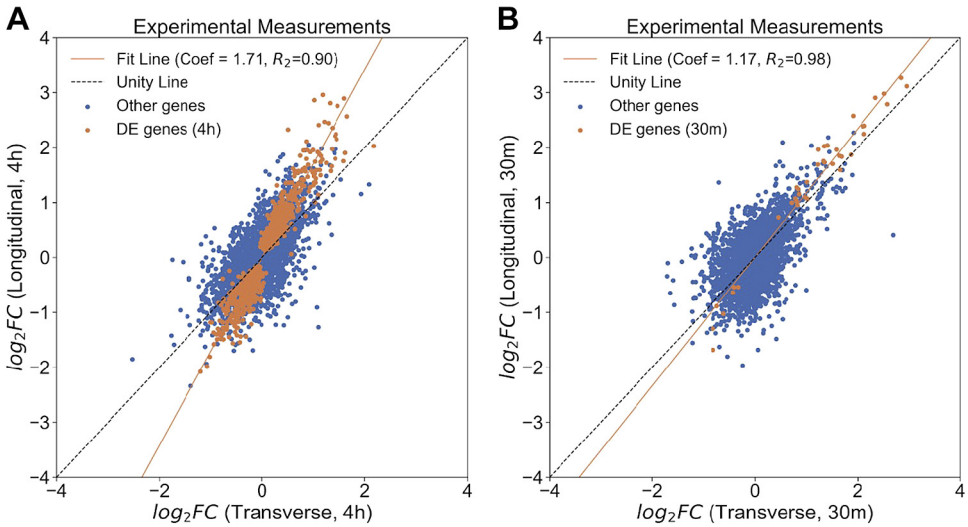

Figure 5. Correlation of gene expression (log_2 fold change) induced by longitudinal vs. transverse stretch. Regression of gene expression induced by longitudinal vs. transverse stretch for 4 h (*A*) and 30 min (*B*) analyzed for genes that were differentially expressed (DE) by either stretch condition (FDR $\leq$ 0.05). Linear regression slopes (Coef) and Pearson coefficients R_2 are shown. Mean log_2 fold changes of 14,861 genes from $n = 3$ technical replicates per stretch group and time point are plotted. FDR, false discovery rate.

AT_1 and Endothelin-1 Receptors Are Key Regulators of Stretch Signaling in Cardiomyocytes

To investigate which pathways in the model are the most important regulators of myocyte stretch responses, each receptor (and one ligand) in the network was individually blocked in the model, and the effect on stretch-regulated expression was computed for each gene for which measured $|\log_2 FC|$ was at least 0.5 for any stretch condition. The model predicted greatest inhibition of stretch-regulated gene expression when the angiotensin II type 1 (AT_1) and endothelin-1 (ET_1) receptors were blocked and least inhibition when the mechanosensitive Trp channel (TRP), L-type calcium channel (LCC), and the sodium hydrogen exchanger (NHE) were blocked (Fig. 7). In the model, the G protein-coupled receptors (GPCR) regulate MAPK signaling, whereas the ion channels and exchanger activate calcium signaling. Then we simulated the effect of combined inhibition of these two groups of receptors. Simulating block of both the AT_1 and ET_1 receptors inhibited stretch-induced expression of over half the activated genes in the model by over 50%, whereas combined inhibition of the LTCC, NHE, and TRP channels caused a median inhibition of less than 20% (Fig. 8*A*). These predictions were tested by RT-PCR measurements that showed a significantly greater inhibition (48%) in the transverse-stretch-induced expression of Ctgf, Fosl2, Mafk, and Nuak1 by combined pharmacological inhibition of AT_1 and ET_1 receptors, compared with 18% measured due to combined inhibition of the LTCC, NHE, and TRP channels (Fig. 8*B*). For four genes (Ctgf, Fosl2, Mafk, and Nuak1) out of six tested, RT-PCR confirmed the model predictions that combination of pharmacological blockade of the AT_1 and ET_1 receptors inhibits stretch-induced gene expression more than blocking the TRP, LTCC, and NHE channels. However, for two genes (Hbegf and Tgfb2), AT_1/ET_1 combination block failed to elicit the model-predicted inhibition of stretch-regulated gene expression (Fig. 8*B*). Network centrality analysis and validation experiments suggest that GPCR activation of MAPK signaling is dominant regulator of gene expression in the model via the activity of nine transcription factors (Fig. 9).

DISCUSSION

Hypertrophic remodeling of cardiomyocytes is regulated by a variety of mechanical stimuli. We and others have shown that cardiac myocyte gene expression is regulated differently by stretch that is primarily parallel to the myofilament axis than by stretch in the transverse direction (8). The anisotropy of myocardial strain in vivo varies with external hemodynamic loading and location in the ventricular wall. We used nonequibiaxial stretching of micropatterned mouse neonatal cardiomyocytes together with a network model of mechanoregulated gene expression to identify signaling pathways and gene expression programs regulated by axis-specific cell strain. Four hours of static longitudinal stretch in vitro induced differential expression of 557 genes, compared with only 30 for the same duration of transverse stretch. However, careful analysis suggested that the main reason for this difference was not strain axis specificity of mechanosignaling. Rather our model and data analysis support the conclusion that, in this model system, cardiomyocytes are at least twice as sensitive to longitudinal stretch as they are to transverse stretch.

Since myocardial systolic and diastolic deformations in vivo are invariably multiaxial (except in papillary muscles and trabeculae), we applied stretch simultaneously along orthogonal axes in a ratio of ~4:1. The anisotropic stretch ratios used in our study approximate those seen during filling. In one study (40), left ventricular free wall longitudinal fiber stretch during filling was transmurally uniform averaging 7%, whereas transverse stretch increased monotonically from 3% on the epicardium to 17% on the subendocardium. Hence, the average transverse stretch during filling in the free wall was also higher than the average longitudinal stretch, which may also underlie the lower sensitivity to transverse stretch that we measured.

The ratio of sensitivities to longitudinal versus transverse stretch that we measured may have been higher had we applied uniaxial stretch along each axis. In an alternative interpretation of our observations, myocytes may have been responding solely to the magnitude of longitudinal strain, with no sensitivity to transverse loading. This upper limit

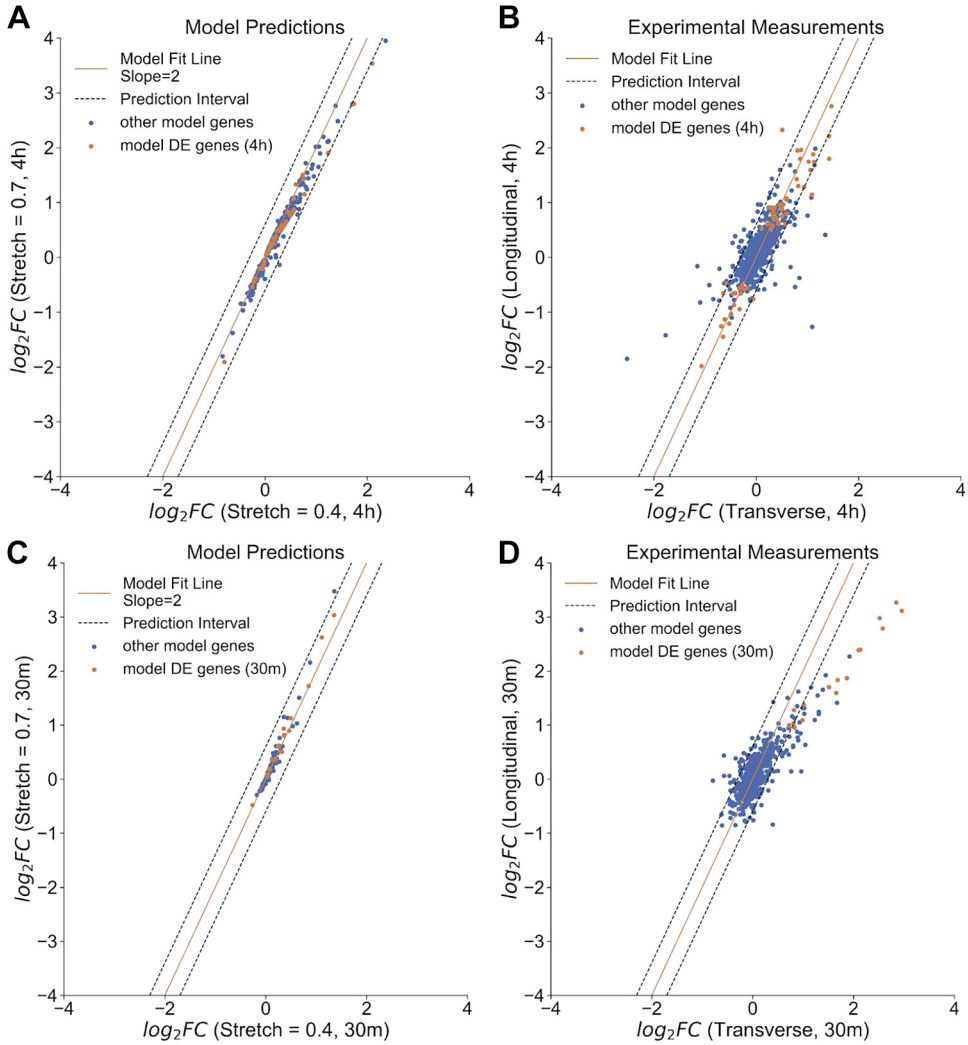

Figure 6. Predicted ratio of gene expression due to longitudinal vs. transverse stretch. *A*: predicted $\log_2$ fold changes of model output genes for 4-h stretch with initial stretch stimuli of 0.7 ("longitudinal") vs. 0.4 ("transverse"). *B*: measured $\log_2$ fold changes of model output genes for 4-h longitudinal vs. 4-h transverse stretch with model slope and 95th percentile range superimposed. Same data as in Fig. 5*A*, but only for genes in the model. *C*: predicted $\log_2$ fold changes of model output genes for 30-min stretch with initial stretch stimuli of 0.7 ("longitudinal") vs. 0.4 ("transverse"). *D*: measured $\log_2$ fold changes of model output genes for 30 min longitudinal vs. 30 min transverse stretch with model-computed slope and 95th percentile range superimposed. Same data as in Fig. 5*B*, but only for genes in the model.

interpretation of our findings seems less probable in the light of previous uniaxial studies, showing that micropatterned neonatal myocytes do respond acutely to static uniaxial stretch applied transversely (41). However, this example serves to demonstrate that more experiments, under a wider range of uniaxial and multiaxial stretch conditions, are required.

The alignment of cardiac myocytes and extracellular matrix in myocardium and the highly organized cytoskeleton of cardiac myocytes make their biophysics, mechanotransmission, and mechanosensing dependent on the localization and axes of physical interactions. Both the *z*-disk and costamere are aligned transversely to the myofilament axis, and both are signaling centers for mechanotransduction (42), though it is not clear which specific physical stimuli these structures are more sensitive to. However, there are possible structural explanations for the findings here. Cardiomyocytes have an extensive membrane cytoskeletal network that supports cortical tension and is thought to be important in determining how externally applied tractions are distributed internally. Kumar et al. (43) found that increased tension on talin in uniaxially stretched cells was independent of the stretch axis relative to the orientation of focal adhesions. When filamin A was knocked down, talin tension became polarized in the direction of stretch. Interestingly, filamin mutations are associated with cardiomyopathies (44).

Several previous studies in cultured rat neonatal ventricular myocytes have reported a more robust response to transverse stretch than longitudinal stretch, typically after 24 h (8). Gopalan et al. (8) observed that 24 h of longitudinal strain in rat neonatal ventricular myocytes did not significantly alter myofibril accumulation or protein expression of hypertrophic markers, but transverse principal strain significantly increased myocyte staining of actin filaments, atrial natriuretic peptide, connexin-43 and *N*-cadherin. The duration of stretch is likely to be important in these experiments. We limited our stretch duration to 4 h based on the observation that cultured micropatterned rodent neonatal ventricular myocytes hypertrophied longitudinally in response to 10% static longitudinal strain fast enough that unstretched sarcomere length was fully restored in 4 h (10), after which myocytes would no longer "feel" the applied stretch. This assembly of new sarcomeres in series was inhibited by blocking PKC and focal adhesion kinase (FAK) signaling (10). To account for this property, our analysis used the "cell area" phenotype output of the model as a feedback variable that

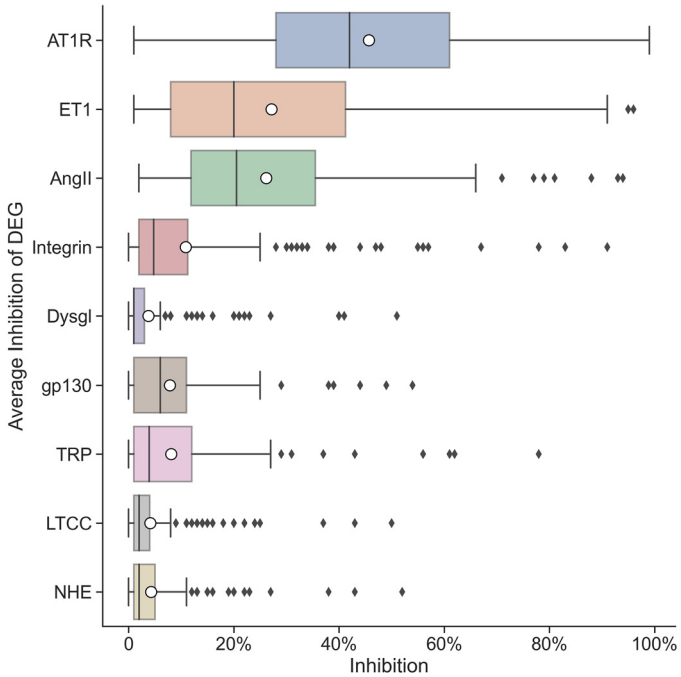

Figure 7. Inhibition of stretch-regulated gene expression by receptor inhibition. Box and whisker plots of percent inhibition of stretch-regulated expression of all genes in the model that changed by $|\log_2 FC| > 0.5$ when each of the 8 receptors and 1 ligand were separately blocked. FC, fold change.

proportionately reduced the effective applied stretch over the duration of simulation, as seen in Fig. 4. The use of dynamic, oscillatory stretching would make it practical to apply longer durations of stretch that could induce more and larger changes in gene expression. Nevertheless, we note that even genes that were not significantly differentially expressed in our analysis nevertheless exhibited a similar significant correlation between fold changes induced by longitudinal versus transverse stretch, as seen in Fig. 5. Our other motivation for choosing short time points was that the signaling model has been validated in greatest detail with shorter time scale experiments before the effects of feedback remodeling of the signaling pathways themselves become significant.

To help interpret the measured transcriptional responses to stretch, we extended our earlier logic-based computational model of the cardiac myocyte mechanosignaling network (12) to incorporate transcriptional control of 784 genes regulated by 11 transcription factors in the network. This novel analysis predicted observed changes in gene expression after 4 h of longitudinal stretch with accuracies of 69–77% for differentially expressed genes. To our knowledge, this is the first model analysis of its kind to predict genome-scale transcriptional responses to mechanical stimulation in any cell type. The gene outputs of the model were also enriched for the same KEGG pathways as the differentially expressed transcripts found with RNA-seq, suggesting that the measurements were consistent with the published literature used to create the model. However, many genes that were significantly induced by stretch were not represented in the model. Differentially expressed genes that were not included in the model were specifically enriched for many other pathways including some known to regulate mechanosignaling and cell-matrix interactions such as Hippo and Rap1 (45–47). Several genes encoding for potassium channels were significantly downregulated with stretch but not included in the model. Downregulation of repolarizing potassium currents is a characteristic of the proarrhythmic electrical remodeling associated with structural heart diseases in which myocardial mechanical loading is increased, such as ventricular hypertrophy and heart failure (48). Although studies have investigated mechanoregulation of the expression of junctional proteins involved in electrical conduction such as connexin-43 (49), mechanoregulated pathways controlling potassium channel remodeling have not been elucidated.

To define key pathways that mediate these stretch responses, we simulated inhibition of all the mechanosensitive receptors in the model and predicted that gene responses induced by either transverse stretch or longitudinal stretch were inhibited most when the AT_1 and ET_1 receptors were blocked. These predictions were partially confirmed by experiments. Sensitivity and network centrality analysis suggested a dominant role for MAPK signaling in regulating nine stretch-regulated transcription factors. In contrast, the three ionic currents in the model and cytosolic calcium signaling had a much smaller total influence.

Boolean and ODE (ordinary differential equation) models of gene expression have been used to help interpret experimental measurements to infer new relationships from data and define new, testable hypotheses. Our network model is based on a logic-based ODE system that uses Hill-type equations for the normalized activity of signaling nodes. Although normalizing the activities of signaling molecules between zero and maximal generally facilitates comparison with experimental measurements, it is much less useful for gene transcription, which is conventionally normalized with respect to a baseline or control that can vary widely between experimental systems. Therefore, we used mass action kinetics to model mRNA synthesis and degradation, by computing mRNA degradation rates from published measurements of gene half-lives and solving for transcription rates that matched control state measurements by assuming steady state at baseline and assuming a linear relationship between gene activation rates and normalized transcription factor activity. Although this approach allowed us to account for measured control of mRNA levels, it also required us to assign an arbitrary residual level of constitutive network activation at baseline. More biochemically realistic models of transcriptional regulation have been developed that could overcome some of the limitations of our current implementation (50).

LIMITATIONS

Our experimental apparatus applies static nonequibiaxial stretch (13). Although many investigators have used pulsatile stretch to better approximate dynamic myocyte loading in vivo, for oscillatory stretch to replicate physiological mechanical conditions, myocytes would also need to be synchronously paced in phase with the stretch, which is rarely done. Instead, we consider the static stretch stimulus to be more representative of the effects of a sustained alteration in

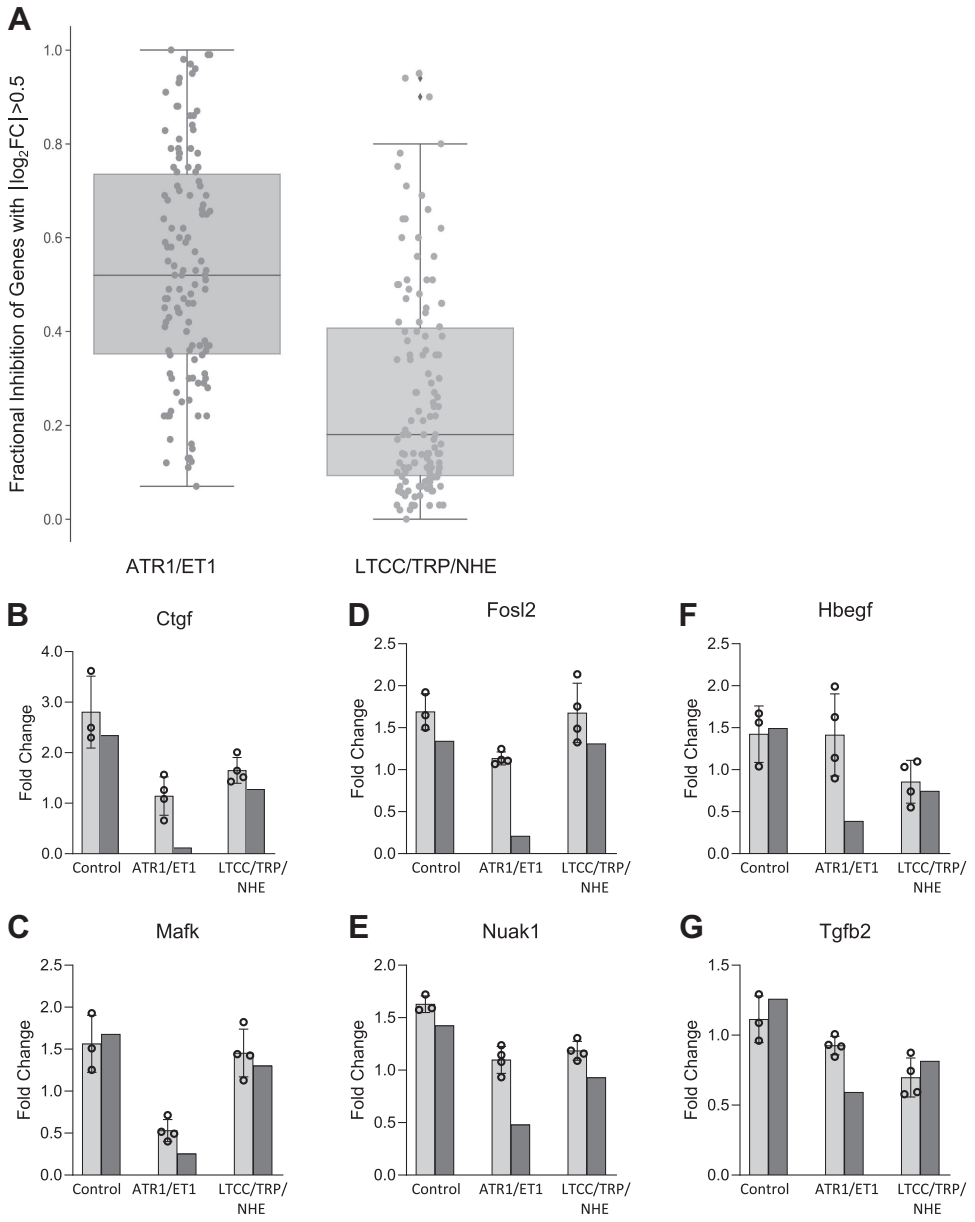

Figure 8. Effects of combination receptor blockade on stretch-induced gene expression. *A*: comparison of predicted changes in stretch-induced expression of genes in the model (for which experimentally measured $|\log_2 FC| > 0.5$) when both the most sensitive receptors [angiotensin II receptor type 1 receptor (AT_1R) and endothelin-1 receptor (ET_1R)] were blocked, compared with when the 3 least sensitive receptors [L-type calcium channel (LTCC), sodium hydrogen exchange (NHE), and Trp channel (TRP)] were all blocked. For 4 genes out of 6, Ctgf (*B*), Mafk (*C*), Fosl2 (*D*), and Nuak1 (*E*), RT-PCR confirmed model predictions that combination of pharmacological blockade of AT_1R and ET_1R inhibits stretch-induced gene expression more than blocking TRP, LTCC, and NHE channels. For Hbegf (*F*) and Tgfb2 (*G*), AT_1R/ET_1R combination block did not result in the predicted degree of inhibition. Error bars show ±1 SD; $n = 4$ technical replicates per group for polymerase chain reaction (PCR) measurements. FC, fold change.

mean hemodynamic loading on the heart. Although the nonequibiaxial cell stretcher we used does apply physiologically representative anisotropic strains, because it was not purely uniaxial, some stretch was simultaneously applied in both directions. The 3.6% longitudinal strain, when the major stretch axis was transverse, may have been sufficient to elicit a response and explain why we could not identify a significant number of genes that were exclusively activated by transverse stretch alone. It is also likely that the short 4-h duration of our study (owing to the decaying nature of the static stretch stimulus discussed earlier) was not long enough to detect responses across the entire cardiac myocyte transcriptome. For example, the comparatively slow mRNA synthesis and processing rates of very long transcripts like the titin N2-A variant in mice probably precluded the detection of statistically significant changes after only 4 h. Indeed, the model itself predicts 183 genes with a $\log_2$ fold change magnitude exceeding 0.5 that had not reached a peak or minimum by 12 h. This finding suggests that even under conditions when the stretch stimulus has subsided by 4 h, experimental measurements for 12 h or longer are needed to more thoroughly test the model.

Additional experimental limitations included that the myocytes used in this study were neonatal rather than mature adult cells and the cultures included nonmyocytes, especially cardiac fibroblasts. Although most previous in vitro studies have also used immature myocyte cultures that tend to be more plastic and adherent than adult cardiac myocytes, the network model was also based on studies in intact adult hearts, such as the transverse aortic constriction model of pressure overload. Our myocytes were purified before culture by preplating, as described previously (13).

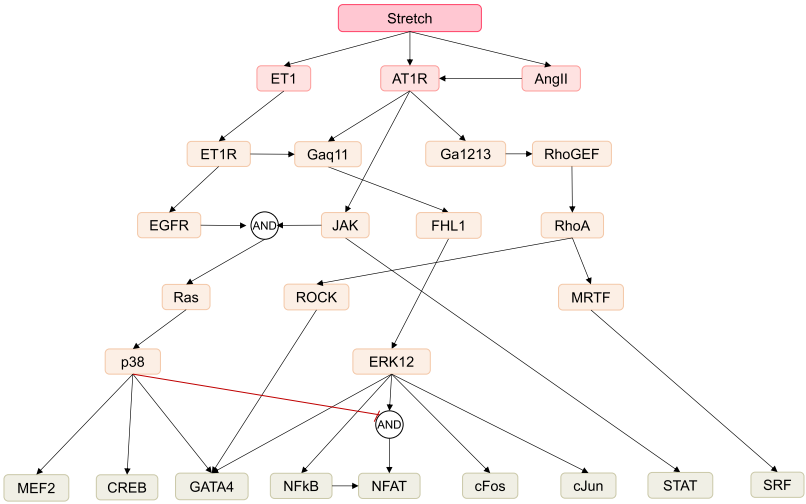

Figure 9. Subnetwork representing the dominant regulators of stretch-induced gene expression in the network model. Derived by network centrality analysis, the subnetwork includes 13 signaling molecules regulating 9 transcription factors.

However, this does not completely remove all nonmyocytes, so some measured transcripts could originate from nonmyocytes or because of paracrine signaling to cardiomyocytes from nonmyocytes. Statistical limitations of the RNA-seq measurements may also contribute to differences between model and experiment. Power analysis of the RNA-seq data yielded a power of 0.8 owing to the relatively small number of biological replicates. Therefore, although the FDR criterion was comparatively stringent, the probability of a type II error was considerably higher. Genes predicted by the model to be stretch-regulated, whose observed changes did not reach statistical significance, would be good candidates for more detailed experimental investigation with more replicates.

Many genes found to be differentially expressed in stretch cardiomyocytes were not included in the model. These missing genes could suggest additional regulatory pathways to add. Some of the literature sources used to construct the transcriptional regulatory network were based on experiments that were not specific to cardiac myocytes, and none of these interactions were specific to stretch. Signaling parameters of the model were mainly derived from our previously published and validated network model without any parameter optimization (12). In a recent uncertainty quantification study of that network model (51), we found that the model accuracy was robust to parameter changes over a wide range. In the present extension to the model, we were able to predict mRNA fold changes over time, enabling more quantitative comparison with experiments. This, coupled with the larger number of model outputs, should make the new model more suitable for numerical parameter optimization. The model also only uses canonical mechanisms of transcriptional regulation. Published studies indicate that other regulatory mechanisms such as microRNAs are also important in myocyte responses to mechanical loading (52, 53). The model tended to overestimate fold changes when there were two or more transcriptional regulators. We found that altering network properties in the transcriptional regulatory model would cause mRNA expression to tend to saturate with more than two to three regulators, consistent with the experimental measurements (Supplemental Fig. S5). Hence, there is potential for parameter optimization to improve the quantitative accuracy of the model. However, here we did not attempt to optimize model parameters.

Conclusions

In this study, we found that micropatterned primary neonatal mouse ventricular myocytes have very different transcriptomic responses to acute strains applied primarily parallel to the myofilament axis compared with transversely applied strains. We investigated these differences using a novel extension of our previous myocyte mechanosignaling model that added the transcriptional regulation of 784 target genes and predicted mechanically regulated transcriptional responses with an overall accuracy of 74–80%. Our analysis suggests that the primary difference between transverse and longitudinal stretch responses in cardiomyocytes may be related to the sensitivity of directional mechanotransduction, rather than the activation of differential signaling pathways by transverse and longitudinal strain. Using combination of inhibitor simulations and experiments, we found that stretch-induced gene expression in neonatal mouse ventricular myocytes is mainly regulated by pathways downstream of the angiotensin II and endothelin-1 receptors, especially MAPK signaling.

DATA AVAILABILITY

All the code and data used to generate results here are in a Jupyter Notebook publicly available on GitHub: https://github.com/cmrglab/GENEode/tree/master/geneode/StretchPaper (10.5281/zenodo.10247058). RNA-seq data are available on GEO (Accession No. GSE83655): https://www.ncbi.nlm.nih.gov/geo/query/acc.cgi?acc=GSE83655.

SUPPLEMENTAL DATA

Supplemental Tables S1–S3 and Supplemental Figs. S1–S5: https://doi.org/10.5281/zenodo.10247058.

ACKNOWLEDGMENTS

Present address of A. D. McCulloch: Depts. of Bioengineering and Medicine, University of California San Diego, La Jolla, CA, United States.

GRANTS

This work was supported by National Institutes of Health Grants HL105242, HL137100, HL122199, HL126273, R01 HL162925, and R01 HL160665 and P41 GM103426 (National Biomedical Computation Resource, to A.D.M.) and Wu Tsai Human Performance Alliance and the Joe and Clara Tsai Foundation.

DISCLOSURES

Andrew D. McCulloch and Jeffrey H. Omens are cofounders of and have equity interests in Insilicomed, Inc., and serve as scientific advisors. Andrew D. McCulloch is also a cofounder of and scientific advisor to Vektor Medical, Inc. Some of their research grants have been identified for conflict-of-interest management based on the overall scope of the project and its potential benefit to these companies. These authors are required to disclose this relationship in publications acknowledging the grant support; however, the research subject and findings reported in this study did not involve the companies in any way and have no relationship with the business activities or scientific interests of either company. The terms of this arrangement have been reviewed and approved by the University of California San Diego in accordance with its conflict-of-interest policies. The manuscript includes a disclosure from Andrew D. McCulloch and Jeffrey H. Omens required by our institution even though there is no connection to the subject matter or materials discussed in this manuscript. None of the other authors has any conflicts of interest, financial or otherwise, to disclose.

AUTHOR CONTRIBUTIONS

S.C., K.S.B., J.H.O., and A.D.M. conceived and designed research; K.S.B. and J.C.S. performed experiments; S.C., K.S.B., P.T., J.C.S., A.F., K.R.K., A.K., A.C.Z., and A.D.M. analyzed data; S.C., K.S.B., A.W., A.C.Z., J.H.O., J.J.S., and A.D.M. interpreted results of experiments; S.C. prepared figures; S.C., A.W., and A.D.M. drafted manuscript; S.C., K.S.B., J.C.S., A.F., K.R.K., A.K., A.C.Z., J.H.O., J.J.S., and A.D.M. edited and revised manuscript; S.C., K.S.B., P.T., J.C.S., A.W., A.F., K.R.K., A.K., A.C.Z., J.H.O., J.J.S., and A.D.M. approved final version of manuscript.

REFERENCES

1. **Grossman W**, **Paulus WJ.** Myocardial stress and hypertrophy: a complex interface between biophysics and cardiac remodeling. *J Clin Invest* 123: 3701–3703, 2013. doi:10.1172/JCI69830.
2. **Lyon RC**, **Zanella F**, **Omens JH**, **Sheikh F.** Mechanotransduction in cardiac hypertrophy and failure. *Circ Res* 116: 1462–1476, 2015. doi:10.1161/CIRCRESAHA.116.304937.
3. **Saucerman JJ**, **Tan PM**, **Buchholz KS**, **McCulloch AD**, **Omens JH.** Mechanical regulation of gene expression in cardiac myocytes and fibroblasts. *Nat Rev Cardiol* 16: 361–378, 2019. doi:10.1038/s41569-019-0155-8.
4. **Lammerding J**, **Kamm RD**, **Lee RT.** Mechanotransduction in cardiac myocytes. *Ann N Y Acad Sci* 1015: 53–70, 2004. doi:10.1196/annals.1302.005.
5. **Sugden PH.** Mechanotransduction in cardiomyocyte hypertrophy. *Circulation* 103: 1375–1377, 2001. doi:10.1161/01.cir.103.10.1375.
6. **Jaalouk DE**, **Lammerding J.** Mechanotransduction gone awry. *Nat Rev Mol Cell Biol* 10: 63–73, 2009. doi:10.1038/nrm2597.
7. **Davis J**, **Davis LC**, **Correll RN**, **Makarewich CA**, **Schwanekamp JA**, **Moussavi-Harami F**, **Wang D**, **York AJ**, **Wu H**, **Houser SR**, **Seidman CE**, **Seidman JG**, **Regnier M**, **Metzger JM**, **Wu JC**, **Molkentin JD.** A tension-based model distinguishes hypertrophic versus dilated cardiomyopathy. *Cell* 165: 1147–1159, 2016. doi:10.1016/j.cell.2016.04.002.
8. **Gopalan SM**, **Flaim C**, **Bhatia SN**, **Hoshijima M**, **Knoell R**, **Chien KR**, **Omens JH**, **McCulloch AD.** Anisotropic stretch-induced hypertrophy in neonatal ventricular myocytes micropatterned on deformable elastomers. *Biotechnol Bioeng* 81: 578–587, 2003. doi:10.1002/bit.10506.
9. **Bullard TA**, **Hastings JL**, **Davis JM**, **Borg TK**, **Price RL.** Altered PKC expression and phosphorylation in response to the nature, direction, and magnitude of mechanical stretch. *Can J Physiol Pharmacol* 85: 243–250, 2007. doi:10.1139/y07-023.
10. **Mansour H**, **de Tombe PP**, **Samarel AM**, **Russell B.** Restoration of resting sarcomere length after uniaxial static strain is regulated by protein kinase Cepsilon and focal adhesion kinase. *Circ Res* 94: 642–649, 2004. doi:10.1161/01.RES.0000121101.32286.C8.
11. **Cingolani HE**, **Ennis IL**, **Aiello EA**, **Pérez NG.** Role of autocrine/paracrine mechanisms in response to myocardial strain. *Pflugers Arch* 462: 29–38, 2011. doi:10.1007/s00424-011-0930-9.
12. **Tan PM**, **Buchholz KS**, **Omens JH**, **McCulloch AD**, **Saucerman JJ.** Predictive model identifies key network regulators of cardiomyocyte mechano-signaling. *PLoS Comput Biol* 13: e1005854, 2017. doi:10.1371/journal.pcbi.1005854.
13. **Camelliti P**, **Gallagher JO**, **Kohl P**, **McCulloch AD.** Micropatterned cell cultures on elastic membranes as an in vitro model of myocardium. *Nat Protoc* 1: 1379–1391, 2006. doi:10.1038/nprot.2006.203.
14. **Pfeiffer ER**, **Wright AT**, **Edwards AG**, **Stowe JC**, **McNall K**, **Tan J**, **Niesman I**, **Patel HH**, **Roth DM**, **Omens JH**, **McCulloch AD.** Caveolae in ventricular myocytes are required for stretch-dependent conduction slowing. *J Mol Cell Cardiol* 76: 265–274, 2014. doi:10.1016/j.yjmcc.2014.09.014.
15. **Wingett SW**, **Andrews S.** FastQ Screen: a tool for multi-genome mapping and quality control. *F1000Res* 7: 1338, 2018. doi:10.12688/f1000research.15931.1.
16. **Kim D**, **Paggi JM**, **Park C**, **Bennett C**, **Salzberg SL.** Graph-based genome alignment and genotyping with HISAT2 and HISAT-genotype. *Nat Biotechnol* 37: 907–915, 2019. doi:10.1038/s41587-019-0201-4.
17. **Liao Y**, **Smyth GK**, **Shi W.** featureCounts: an effcient general purpose program for assigning sequence reads to genomic features. *Bioinformatics* 30: 923–930, 2014. doi:10.1093/bioinformatics/btt656.
18. **Love MI**, **Huber W**, **Anders S.** Moderated estimation of fold change and dispersion for RNA-seq data with DESeq2. *Genome Biol* 15: 550, 2014. doi:10.1186/s13059-014-0550-8.
19. **Huang da W**, **Sherman BT**, **Lempicki RA.** Systematic and integrative analysis of large gene lists using DAVID bioinformatics resources. *Nat Protoc* 4: 44–57, 2009. doi:10.1038/nprot.2008.211.
20. **Chen J**, **Bardes EE**, **Aronow BJ**, **Jegga AG.** ToppGene Suite for gene list enrichment analysis and candidate gene prioritization. *Nucleic Acids Res* 37: W305–W311, 2009. doi:10.1093/nar/gkp427.
21. **Deivasikamani V**, **Dhayalan S**, **Abudushalamu Y**, **Mughal R**, **Visnagri A**, **Cuthbertson K**, **Scragg JL**, **Munsey TS**, **Viswambharan H**, **Muraki K**, **Foster R**, **Sivaprasadarao A**, **Kearney MT**, **Beech DJ**, **Sukumar P.** Piezo1 channel activation mimics high glucose as a stimulator of insulin release. *Sci Rep* 9: 16876, 2019. doi:10.1038/s41598-019-51518-w.
22. **Shannon P**, **Markiel A**, **Ozier O**, **Baliga NS**, **Wang JT**, **Ramage D**, **Amin N**, **Schwikowski B**, **Ideker T.** Cytoscape: a software environment for integrated models of biomolecular interaction networks. *Genome Res* 13: 2498–2504, 2003. doi:10.1101/gr.1239303.
23. **Ryall KA**, **Holland DO**, **Delaney KA**, **Kraeutler MJ**, **Parker AJ**, **Saucerman JJ.** Network reconstruction and systems analysis of cardiac myocyte hypertrophy signaling. *J Biol Chem* 287: 42259–42268, 2012. doi:10.1074/jbc.M112.382937.
24. **Lal H**, **Verma SK**, **Smith M**, **Guleria RS**, **Lu G**, **Foster DM**, **Dostal DE.** Stretch-induced MAP kinase activation in cardiac myocytes: differential regulation through beta1-integrin and focal adhesion kinase. *J Mol Cell Cardiol* 43: 137–147, 2007. doi:10.1016/j.yjmcc.2007.05.012.
25. **Sharova LV**, **Sharov AA**, **Nedorezov T**, **Piao Y**, **Shaik N**, **Ko MS.** Database for mRNA half-life of 19 977 genes obtained by DNA microarray analysis of pluripotent and differentiating mouse embryonic stem cells. *DNA Res* 16: 45–58, 2008. doi:10.1093/dnares/dsn030.
26. **Ben-Tabou de-Leon S**, **Davidson EH.** Modeling the dynamics of transcriptional gene regulatory networks for animal development. *Dev Biol* 325: 317–328, 2009. doi:10.1016/j.ydbio.2008.10.043.
27. **Janky R**, **Verfaillie A**, **Imrichová H**, **Van de Sande B**, **Standaert L**, **Christiaens V**, **Hulselmans G**, **Herten K**, **Naval Sanchez M**, **Potier D**, **Svetlichnyy D**, **Kalender Atak Z**, **Fiers M**, **Marine JC**, **Aerts S.** iRegulon: from a gene list to a gene regulatory network

using large motif and track collections. *PLoS Comput Biol* 10: e1003731, 2014. doi:10.1371/journal.pcbi.1003731.
28. **Wingender E**, **Chen X**, **Fricke E**, **Geffers R**, **Hehl R**, **Liebich I**, **Krull M**, **Matys V**, **Michael H**, **Ohnhäuser R**, **Prüss M**, **Schacherer F**, **Thiele S**, **Urbach S.** The TRANSFAC system on gene expression regulation. *Nucleic Acids Res* 29: 281–283, 2001. doi:10.1093/nar/29.1.281.
29. **Bryne JC**, **Valen E**, **Tang MH**, **Marstrand T**, **Winther O**, **da Piedade I**, **Krogh A**, **Lenhard B**, **Sandelin A.** JASPAR, the open access database of transcription factor-binding profiles: new content and tools in the 2008 update. *Nucleic acids Res* 36: D102–D106, 2007. doi:10.1093/nar/gkm955.
30. **Hume MA**, **Barrera LA**, **Gisselbrecht SS**, **Bulyk ML.** UniPROBE, update 2015: new tools and content for the online database of protein-binding microarray data on protein-DNA interactions. *Nucleic Acids Res* 43: D117–22, 2015. doi:10.1093/nar/gku1045.
31. **Koschützki D**, **Schreiber F.** Centrality analysis methods for biological networks and their application to gene regulatory networks. *Gene Regul Syst Bio* 2: 193–201, 2008. doi:10.4137/grsb.s702.
32. **Yoon J**, **Blumer A**, **Lee K.** An algorithm for modularity analysis of directed and weighted biological networks based on edge-betweenness centrality. *Bioinformatics* 22: 3106–3108, 2006. doi:10.1093/bioinformatics/btl533.
33. **Benjamini Y**, **Hochberg Y.** Controlling the false discovery rate: a practical and powerful approach to multiple testing. *J R Stat Soc Ser B Methodol* 57: 289–300, 1995. doi:10.1111/j.2517-6161.1995.tb02031.x.
34. **Robinson MD**, **McCarthy DJ**, **Smyth GK.** edgeR: a bioconductor package for differential expression analysis of digital gene expression data. *Bioinformatics* 26: 139–140, 2010. doi:10.1093/bioinformatics/btp616.
35. **Bi R**, **Liu P.** Sample size calculation while controlling false discovery rate for differential expression analysis with RNA-sequencing experiments. *BMC Bioinformatics* 17: 146, 2016. doi:10.1186/s12859-016-0994-9.
36. **Müllner D.** Modern hierarchical, agglomerative clustering algorithms (Preprint). *arXiv* 1109.2378, 2011. doi:10.48550/arXiv.1109.2378.
37. **Bar-Joseph Z**, **Gifford DK**, **Jaakkola TS.** Fast optimal leaf ordering for hierarchical clustering. *Bioinformatics* 17, Suppl 1: S22–S29, 2001. doi:10.1093/bioinformatics/17.suppl_1.s22.
38. **Rysä J**, **Tokola H**, **Ruskoaho H.** Mechanical stretch induced transcriptomic profiles in cardiac myocytes. *Sci Rep* 8: 1–14, 2018. doi:10.1038/s41598-018-23042-w.
39. **Wang Y**, **Zhang Y**, **Ding G**, **May HI**, **Xu J**, **Gillette TG**, **Wang H**, **Wang ZV.** Temporal dynamics of cardiac hypertrophic growth in response to pressure overload. *Am J Physiol Heart Circ Physiol* 313: H1119–H1129, 2017. doi:10.1152/ajpheart.00284.2017.
40. **Omens JH**, **May KD**, **McCulloch AD.** Transmural distribution of three-dimensional strain in the isolated arrested canine left ventricle. *Am J Physiol Heart Circ Physiol* 261: H918–H928, 1991. doi:10.1152/ajpheart.1991.261.3.H918.
41. **Yang H**, **Schmidt LP**, **Wang Z**, **Yang X**, **Shao Y**, **Borg TK**, **Markwald R**, **Runyan R**, **Gao BZ.** Dynamic myofibrillar remodeling in live cardiomyocytes under static stretch. *Sci Rep*. 6: 20674, 2016. doi:10.1038/srep20674.
42. **Pyle WG**, **Solaro RJ.** At the crossroads of myocardial signaling: the role of Z-discs in intracellular signaling and cardiac function. *Circ Res* 94: 296–305, 2004. doi:10.1161/01.RES.0000116143.74830.A9.
43. **Kumar A**, **Shutova MS**, **Tanaka K**, **Iwamoto DV**, **Calderwood DA**, **Svitkina TM**, **Schwartz MA.** Filamin A mediates isotropic distribution of applied force across the actin network. *J Cell Biol* 218: 2481–2491, 2019. doi:10.1083/jcb.201901086.
44. **Song S**, **Shi A**, **Lian H**, **Hu S**, **Nie Y.** Filamin C in cardiomyopathy: from physiological roles to DNA variants. *Heart Fail Rev* 27: 1373–1385, 2022. doi:10.1007/s10741-021-10172-z.
45. **Windmueller R**, **Morrisey EE.** Hippo and cardiac hypertrophy: a complex interaction. *Circ Res* 117: 832–834, 2015. doi:10.1161/CIRCRESAHA.115.307546.
46. **Tian Y**, **Liu Y**, **Wang T**, **Zhou N**, **Kong J**, **Chen L**, **Snitow M**, **Morley M**, **Li D**, **Petrenko N**, **Zhou S**, **Lu M**, **Gao E**, **Koch WJ**, **Stewart KM**, **Morrisey EE.** A microRNA-Hippo pathway that promotes cardiomyocyte proliferation and cardiac regeneration in mice. *Sci Transl Med* 7: 279ra38, 2015. doi:10.1126/scitranslmed.3010841.
47. **Jeyaraj SC**, **Unger NT**, **Chotani MA.** Rap1 GTPases: an emerging role in the cardiovasculature. *Life Sci* 88: 645–652, 2011. doi:10.1016/j.lfs.2011.01.023.
48. **Cutler MJ**, **Jeyaraj D**, **Rosenbaum DS.** Cardiac electrical remodeling in health and disease. *Trends Pharmacol Sci* 32: 174–180, 2011. doi:10.1016/j.tips.2010.12.001.
49. **Yamada K**, **Green KG**, **Samarel AM**, **Saffitz JE.** Distinct pathways regulate expression of cardiac electrical and mechanical junction proteins in response to stretch. *Circ Res* 97: 346–353, 2005. doi:10.1161/01.RES.0000178788.76568.8a.
50. **Ay A**, **Arnosti DN.** Mathematical modeling of gene expression: a guide for the perplexed biologist. *Crit Rev Biochem Mol Biol* 46: 137–151, 2011. doi:10.3109/10409238.2011.556597.
51. **Cao S**, **Aboelkassem Y**, **Wang A**, **Valdez-Jasso D**, **Saucerman JJ**, **Omens JH**, **McCulloch AD.** Quantification of model and data uncertainty in a network analysis of cardiac myocyte mechanosignalling. *Philos Trans A Math Phys Eng Sci* 378: 20190336, 2020. doi:10.1098/rsta.2019.0336.
52. **Wang N**, **Zhou Z**, **Liao X**, **Zhang T.** Role of microRNAs in cardiac hypertrophy and heart failure. *IUBMB Life* 61: 566–571, 2009. doi:10.1002/iub.204.
53. **Wang J**, **Yang X.** The function of miRNA in cardiac hypertrophy. *Cell Mol Life Sci* 69: 3561–3570, 2012. doi:10.1007/s00018-012-1126-y.